

HLA-E Allelic Variants

CORRELATING DIFFERENTIAL EXPRESSION, PEPTIDE AFFINITIES, CRYSTAL STRUCTURES, AND THERMAL STABILITIES*

Received for publication, August 13, 2002, and in revised form, October 28, 2002
Published, JBC Papers in Press, October 30, 2002, DOI 10.1074/jbc.M208268200

Roland K. Strong^{‡§}, Margaret A. Holmes[‡], Pingwei Li[‡], Laura Braun[¶], Ni Lee[¶],
and Daniel E. Geraghty^{¶||}

From the [‡]Division of Basic Sciences and the [¶]Clinical Research Division, Fred Hutchinson Cancer Research Center, Seattle, Washington 98109

Previous studies of HLA-E allelic polymorphism have indicated that balancing selection may be acting to maintain two major alleles in most populations, indicating that a functional difference may exist between the alleles. The alleles differ at only one amino acid position, where an arginine at position 107 in HLA-E*0101 (E^R) is replaced by a glycine in HLA-E*0103 (E^G). To investigate possible functional differences, we have undertaken a study of the physical and biochemical properties of these two proteins. By comparing expression levels, we found that whereas steady-state protein levels were similar, the two alleles did in fact differ with respect to cell surface levels. To help explain this difference, we undertook studies of the relative differences in peptide affinity, complex stability, and three-dimensional structure between the alleles. The crystal structures for HLA-E^G complexed with two distinct peptides were determined, and both were compared with the HLA-E^R structure. No significant differences in the structure of HLA-E were induced as a result of binding different peptides or by the allelic substitution at position 107. However, there were clear differences in the relative affinity for peptide of each heavy chain, which correlated with and may be explained by differences between their thermal stabilities. These differences were completely consistent with the relative levels of the HLA-E alleles on the cell surface and may indeed correlate with functional differences. This in turn may help explain the apparent balancing selection acting on this locus.

The major histocompatibility complex (MHC)¹ in humans includes the HLA loci, a group of genes encoding glycoproteins

that control cell-to-cell interactions and regulate immune responses. These include the classical class I loci HLA-A, -B, and -C, whose role in immunological recognition is now well understood (1). In addition to these genes, the MHC contains three highly homologous, nonclassical class I genes, HLA-E, -F, and -G, each of which probably plays a specialized role in the immune response. All three genes are located in relatively close proximity within the class I region and together with the classical class I antigens constitute the complete list of active class I genes in humans (2). The remainder of the class I-like sequences are apparently pseudogenes (e.g. HLA-H), gene fragments, and other inactive but structurally homologous sequences. Each of the nonclassical class I genes can be distinguished from classical class I genes by their expression levels, as is the case for HLA-E, which is ubiquitously expressed but at much lower relative levels (3), or by their tissue-specific expression patterns in the case of HLA-G (4) and HLA-F (5, 6). Each is hypothesized to have a unique function in immune responses.

Of the three nonclassical class I genes, the function of HLA-E has been the most completely elucidated through its interaction with CD94-NKG2 receptors (3, 7). CD94 is a type II glycoprotein that is expressed on most NK cells and a subset of T lymphocytes (8, 9). It forms a heterodimer with the NKG2A/B, NKG2C, NKG2E, and NKG2H glycoproteins (10, 11). Interaction with such CD94 heterodimers can augment, inhibit, or have no effect on NK cell-mediated cytotoxicity and cytokine production (12). Surface expression of HLA-E requires, and is therefore controlled by, the availability of any of a set of highly conserved nonamer peptides that are available from the signal sequences of other HLA class I molecules including HLA-A, -B, -C, and -G but not HLA-F (13). When peptide is available, the resultant complex can interact normally with the CD94-NKG2 complex (3, 7). Further, the ability of HLA-E complexes to interact with CD94-NKG2 ligands is affected by the particular nonamer that is available for binding. For example, HLA-E may gain a novel function when it binds the unique peptide that only HLA-G can provide (14). Since HLA-E is also expressed in those placental cells normally expressing HLA-G, such a potentially activating function is suggestive of a unique role that HLA-E might be playing in the placenta.

Polymorphism among HLA class I antigens has long been thought of as a hallmark of the functional diversity required of these molecules (15). Whereas high levels of polymorphism in HLA class I have been maintained by overdominant selection (16), in contrast the nonclassical class I molecules HLA-E, -F, and -G have been under a distinct selective pressure, exhibiting very low levels of allelic polymorphism. Two nonsynonymous alleles of HLA-E have been found, E*0101 and E*0103 (17, 18),

* This work was supported by National Institutes of Health (NIH) Grant R01 AI48675 and the Pendleton Fund (to R. K. S.) and by NIH Grants R01 AI38508 and AI49213 (to D. E. G.). The costs of publication of this article were defrayed in part by the payment of page charges. This article must therefore be hereby marked "advertisement" in accordance with 18 U.S.C. Section 1734 solely to indicate this fact.

The atomic coordinates and structure factors (code 1KPR and 1KTL) have been deposited in the Protein Data Bank, Research Collaboratory for Structural Bioinformatics, Rutgers University, New Brunswick, NJ (<http://www.rcsb.org/>).

§ To whom correspondence may be addressed: Fred Hutchinson Cancer Research Center, 1100 Fairview Ave. N., A3-023, Seattle, WA 98109. Tel.: 206-667-5587; Fax: 206-667-6877; E-mail: rstrong@fhcr.org.

|| To whom correspondence may be addressed: Fred Hutchinson Cancer Research Center, 1100 Fairview Ave. N., D4-100, Seattle, WA 98109. Tel.: 206-667-4668; Fax: 206-667-6948; E-mail: geraghty@fhcr.org.

¹ The abbreviations used are: MHC, major histocompatibility complex; β_2m , β_2 -microglobulin; MES, 4-morpholineethanesulfonic acid; Pipes, 1,4-piperazinediethanesulfonic acid; NK, natural killer; FACS, fluorescence-activated cell sorting; LCL, lymphoblastoid cell line.

and although others have been reported, it appears likely that they are the result of sequencing artifacts (19). The two confirmed HLA-E alleles have been referred to as HLA-E^G (E*0101) and HLA-E^R (E*0103), since they are distinguished by having either an arginine (-E^R) or a glycine (-E^G) at position 107 of the protein, located on a loop between β -strands in the $\alpha 2$ domain of the heavy chain. HLA-E^G and -E^R are found at nearly equal frequencies in diverse populations. Evidence that some form of balancing selection is acting on this gene to maintain the two alleles of HLA-E has been reported (20). Such selection would imply that there are functional differences between the two alleles.

In order to investigate the underlying rationale for potential functional differences, we examined the two HLA-E alleles individually for various characteristics that might affect function. Preliminary evidence had indicated that different levels of surface expression of HLA-E could alter its ability to protect cells from NK lysis by NKL cells (3).² Therefore, we examined the HLA-E alleles for differential surface expression levels and, having found evidence for this, undertook experiments to understand the physical basis for these differences. By comparing differences in peptide affinity, three-dimensional structure, and thermal stability of the HLA-E^G and -E^R in complex with various peptides, we were able to elucidate important differences in the physical characteristics of these molecules that may form the basis underlying the effective balancing selection that appears to have been acting on this locus.

MATERIALS AND METHODS

Cell Culture—LCL 721.221 was obtained from the ATCC and maintained in RPMI 1640 medium supplemented with 10% (v/v) fetal calf serum, 2 mM L-glutamine, and 1 mM sodium pyruvate. Transfectants were established by electroporation using the pNS vector followed by G418 selection at 0.8 mg/ml.

Construction of Plasmid, Protein Expression, and Refolding—DNA coding for a glycine-serine linker and a BirA substrate peptide (21) was fused to DNA encoding the HLA-E^G or -E^R heavy chains by PCR with the 5'-primer (CGCGCAATTCAGGAGGAATTTAAAATGGGCTCCC-ACTCCTTG and the 3'-primer (GCGCAAGCTTTTAAACGATGATCC-ACACCATTTTCTGTGCATCCAGAATATGATGCAGGGATCCCGGCT-TCCATCTCAGGGTGACGGGCTCG containing the underlined *EcoRI* and *HindIII* restriction sites, respectively. The 5' primer also contained a ribosomal binding site, a translational spacer element, an N-terminal Met, and the first 5 amino acids of HLA-E exon 2. PCR products were ligated into pHN1+ vector (22) and expressed in *Escherichia coli* strain UBS (23). β_2 -Microglobulin (β_2m) in pHN1+ was kindly provided by D. C. Wiley (Harvard University, Cambridge, MA) and expressed in *E. coli* strain XA90.

Both heavy and light chain (β_2m) inclusion bodies were isolated from cell pellets, washed repeatedly in detergent, and solubilized in 8 M urea, 25 mM MES, pH 6.0, 10 mM EDTA, and 0.1 mM dithiothreitol (solubilization buffer) as described (24). Refolding was accomplished using a variation of the method of O'Callaghan and co-workers (25) by dilution of 12 mg of β_2m (in 2 ml of solubilization buffer) into 500 ml of 400 mM L-arginine, 100 mM Tris, pH 8.0, 2 mM EDTA, 0.5 mM oxidized glutathione, 5 mM reduced glutathione, and 0.2 mM phenylmethylsulfonyl fluoride (refolding buffer). After 1 h at 4 °C, 18.5 mg of heavy chain (in 30 ml of solubilization buffer) and 17 mg of peptide (in Me₂SO at 1.7 mg/ml) were added. The initial molar ratio of heavy chain/ β_2m /peptide was 1:2:30. The refolding mixture was pulsed three times with additional heavy chain at 12-h intervals. After 48 h, the refolding mixture was concentrated initially on a stir cell (Amicon, Beverly, MA) and subsequently in a 10-kDa cut-off Centriprep ultrafiltration unit (Amicon). Refolded HLA-E was separated from aggregates and buffer exchanged into 50 mM Pipes, pH 7.0, 150 NaCl, 1 mM EDTA, and 0.02% Na₂S₂O₃ on a Superdex 75 prep-grade size exclusion chromatography column (Amersham Biosciences).

Construction of pNS Vector Expressing Fusion Proteins—HLA-E^R (E*0101) and HLA-E^G (E*0103) cDNAs were prepared from RNA using B-LCL E^R or E^G homozygotes by reverse transcriptase and PCR as described (26). The mature full-length proteins were fused to exon 1 of

HLA-A2, -B27, -C7, -C14, -C15, or -G, respectively, using PCR and appropriately designed primers, and the chimeric cDNAs were then cloned into the pNS vector (27).

Immunofluorescence Staining and FACS Analysis—Cell surface expression of different HLA-E constructs was measured by indirect immunofluorescence staining as previously described (13). Briefly, cells were preincubated with a saturating concentration of monoclonal antibody 3D12 followed by washing and labeling with fluorescein isothiocyanate-conjugated goat F(ab')₂ anti-mouse Ig (BioSource, Camarillo, CA). Samples were analyzed on a FACScan cytometer (Becton Dickinson, Mountain View, CA).

Measurement of Relative Peptide Affinities—Peptide binding to HLA-E^G and -E^R was compared and quantified using a sandwich enzyme-linked immunosorbent assay method essentially similar to that recently described (28). Briefly, polystyrene (96-well) plates were coated with 100 μ l of HLA-E-specific monoclonal antibody 3D12 (13) diluted in sodium carbonate buffer (pH 9.6) at a concentration of 20 μ g/ml. 100 μ l of HLA-E folded with different peptides at 1:250 dilution in 2% bovine serum albumin/phosphate-buffered saline was added into each well after the excess of the coating monoclonal antibody was removed, and the uncoupled sites were blocked with 5% skim milk in phosphate-buffered saline. Plates were incubated for 1 h at room temperature and washed three times with 0.05% (v/v) Tween 20 in phosphate-buffered saline. After a 1-h incubation of 0.2 μ g/ml peroxidase-conjugated rabbit anti-human β_2m (Dako) in 2% bovine serum albumin/phosphate-buffered saline, plates were washed, and 100 μ l of tetramethyl benzidine substrate (BioSource) was added into each well. 15-min incubation at room temperature was stopped by adding 100 μ l of 2 M H₂SO₄ into each well.

To measure peptide-dependent refolding of HLA-E, 2 M of β_2m was refolded with 1 M heavy chain and peptide at various concentrations as the refolding condition described above, except the refolding mixtures were reacted for 1 h at 4 °C. The relative amount of HLA-E refolded in the presence and absence of added peptide was quantified and compared with maximum assembly achieved using 100 μ M VMAPRTLVL (the HLA-B7 nonamer). Peptide concentrations yielding half-maximum assembly were read directly from the curve and used to compare relative binding to E^G and E^R. This assay thus gives an indirect estimate of relative affinity as described (28).

Western Blotting and Immunodetection—Total cell lysate was prepared and separated on a 14% Tris-glycine gel (Novex, San Diego, CA) and electroblotted as described (13). HLA-E protein was detected by monoclonal antibody 7G3 followed by horseradish peroxidase-labeled goat anti-mouse Igs (BioSource) at 1:5,000 dilution and finally with an enhanced chemiluminescence system (ECL; Amersham Biosciences). Densitometry was performed by scanning the x-ray film with a Sharp JX-320 scanner and quantified with ImageQuant 5.0 software (University of Virginia ITC-Academic Computing Health Sciences).

CD Thermal Denaturation Curves—Data were collected with an AVIV 62A DS CD spectropolarimeter equipped with a thermoelectric cell holder. Samples consisted of 7 μ M protein buffered to a pH of 7.0 with 10 mM potassium phosphate. Thermal denaturation curves were collected at 219 nm, the wavelength of the maximal difference between native and denatured protein CD spectra, over a temperature range of 25–85 °C using a 1-cm path length cuvette. The time constant was 1 s, averaging time was 15 s, and equilibration time was 30 s with a bandwidth of 1 nm. All curves were normalized to a single reference curve by application of a simple scalar multiplier. Each curve represents the point-by-point average of three separate denaturation runs, averaged after normalization. Melting temperatures (T_m) were estimated as the inflection point of polynomials fitted to the averaged curves; we estimate the accuracy of these measurements to be within 0.5 °C.

Crystallization and X-ray Crystallography—Crystals of HLA-E^G with the HLA-B7 nonamer (VMAPRTLVL; E^G-B7) or HLA-E^G with the HLA-B27 peptide (VTAPRTLLL; E^G-B27) were grown by vapor diffusion at 22 °C over a reservoir of 2.2 M (NH₄)₂SO₄, 2% PEG ($M_r = 400$) and 100 mM Tris (pH 8.0), conditions similar to those of O'Callaghan and co-workers (25). Crystals were cryopreserved for data collection by using a mother liquor with 30% (w/w) sucrose. The E^G-B7 data set was collected at -170 °C at beamline 5.0.2 at the Advanced Light Source (Lawrence Berkeley National Laboratory, Berkeley, CA). The E^G-B27 data set was collected at -170 °C on an in-house Rigaku Raxis IV area detector. There are two molecules per asymmetric unit for both complexes. Diffraction data were processed with DENZO and SCALEPACK (29) (see Table I).

Since the E^G-B7 crystals were nearly isomorphous to the original E^R-B7 crystals (25), the coordinates (Brookhaven Protein Data Bank

² N. Lee, unpublished results.

TABLE I
Crystallographic statistics

Values for the highest resolution shell are shown in parentheses. $R_{\text{sym}} \equiv \sum |I - \langle I \rangle| / \sum I$, where I is the observed intensity and $\langle I \rangle$ is the mean intensity of multiple observations of symmetry-related reflections. R_{cryst} , $R_{\text{free}} \equiv \sum \|F_o\| - \|F_c\| / \sum \|F_o\|$ where F_o and F_c are the observed and calculated structure factor amplitudes. R_{free} is calculated from a randomly chosen 10% of the HLA-E^G/B7 reflections excluded from refinement (33). Ramachandran values were calculated with PROCHECK (49). Superpositions were calculated on all common C α s: 382 for E^R/E^R and E^R/E^G comparisons and 383 for E^G/E^G comparisons. rmsd, root mean square deviation.

	HLA-E ^G /B7	HLA-E ^G /B27				
Peptide sequence	VMAPRTVLL	VTAPRTLLL				
Data collection						
Space group	P3 ₁ 21	P3 ₁ 21				
Lattice constants (Å)	$a = b = 178.7; c = 88.2$	$a = b = 178.4; c = 87.3$				
Resolution (Å)	20–2.8 (2.9–2.8)	25–3.1 (3.15–3.1)				
Observations	299,482	265,243				
Unique reflections	38,312	27,568				
Completeness (%)	95.8 (97.3)	94.2 (84.1)				
$I/\sigma(I)$	13.4 (3.1)	19.4 (2.1)				
R_{sym} (%)	5.2 (37.9)	5.9 (41.8)				
Refinement						
Reflections (all $F > 0$)	32,914 (3,672)	23,971 (2,528)				
Protein atoms	6,205	6,210				
Heteroatoms	5	5				
Average group B-factor (Å ²)	63.9	63.0				
$R_{\text{cryst}}/R_{\text{free}}$ (%)	23.5/28.9	23.8 / 28.0				
Geometry (rmsd from ideality)						
Bonds (Å)	0.028	0.027				
Bond angles (degrees)	2.6	2.6				
Dihedral angles (degrees)	27.2	26.9				
Ramachandran						
Most favored (%)	83.3	85.7				
Disallowed (%)	0	0				
Superposition rmsds (Å)						
	E ^R /B7 (1)	E ^R /B7 (2)	E ^G /B7 (1)	E ^G /B7 (2)	E ^G /B27 (1)	E ^G /B27 (2)
E ^R /B7 (1)		0.30	0.66	0.84	0.64	0.79
E ^R /B7 (2)			0.71	0.78	0.70	0.73
E ^G /B7 (1)				0.85	0.11	0.80
E ^G /B7 (2)					0.85	0.17
E ^G /B27 (1)						0.81
E ^G /B27 (2)						

(30) file 1mhe), stripped of waters and the side chain of residue 107, were fitted by rigid body refinement using the CNS software package (31). The model was rebuilt using the xfit module in XtalView (32) against a composite omit map calculated in CNS. Simulated annealing torsional refinement, using the maximum likelihood target function mlf in CNS, was followed by alternating rounds of rebuilding, positional (using the mlf target function), and group B-factor refinement. The progress of the refinement was confirmed by the monotonic decrease in both R_{cryst} and R_{free} (33). Loose noncrystallographic symmetry restraints were applied globally until it was realized that one loop differed between molecules in the asymmetric unit, when noncrystallographic symmetry restraints were removed from that loop. The electron density maps were clear, unambiguous, and readily interpretable except in regions where residues have been built as glycines or alanines due to poor side chain density: heavy chain residues 17 (molecule 1 only), 54, 176, 196, 225 (molecule 2 only), 226 (molecule 2 only), and 256 and β_2 m residues 19 and 75. Building and refinement of the E^G/B27 structure proceeded by a similar protocol except that the E^G-B7 structure was used as the starting point. In order to maintain the independence of the test set, the test reflections for this data set were matched to the E^G-B7 test reflections (34). Both structures include a single ordered sulfate molecule bound between platform domains. The same side chains are missing as for HLA-E^G-B7, except that α -chain residue 226 of molecule 2 has been modeled. Both structures include interpretable density for residue 1, not visualizable in the HLA-E^R structures. Refinement statistics for both structures are given in Table I.

RESULTS

HLA-E Alleles Are Differentially Expressed at the Cell Surface—In previous studies of HLA-E allelic distribution, it was hypothesized that balancing selection might be acting on the two HLA-E alleles, possibly reflecting a functional difference between them (20). In this regard, it was noteworthy that HLA-E allelic variation greatly affected the intracellular transport and cell surface expression of HLA-E when transfected

into mouse cells (35). In order to gain further insight into what distinguishes the HLA-E^G and -E^R complexes, we constructed a set of hybrid genes similar to that previously described (13). Each of these hybrid genes contained the signal sequence derived from an HLA-A, -B, -C, or -G gene physically connected to the HLA-E^G or -E^R mature protein coding sequences. The HLA signal sequence nonamers available for binding to HLA-E by each of these constructs were representative of those widely available in populations. In addition, the B27 nonamer has been shown to bind poorly to the HLA-E^R protein, and the HLA-C7- and HLA-G-derived nonamers have been shown to interact differentially with the CD94-NKG2 ligands (14). Thus, a representative set of HLA-E-nonamer peptide complexes was available for comparison as discrete complexes.

Each of these cDNA constructs was cloned into vector pNS and expressed in 721.221 cells in order to look first at the expression levels both intracellularly and on the cell surface. Fig. 1 shows the results of FACS analysis, which showed that in every case of peptide-HLA-E complex formed, the E^R complex appeared at lower surface levels than did E^G. This was most pronounced in the case of the B27-derived nonamer, since little or no HLA-E^R complex was expressed on the surface of these cells. These differences were apparently not due to lower overall levels of HLA-E protein in these cells as evidenced by Western analysis measuring relative levels of the two allelic heavy chains as roughly equal (Fig. 1, *bottom*). The small differences that were apparent from this measure were significantly less than those measured on the cell surface (*e.g.* B27).

Whereas the transfected hybrid constructs allowed us to measure the relative expression levels of HLA-E^R and -E^G with individual peptides, we examined the relative expression levels

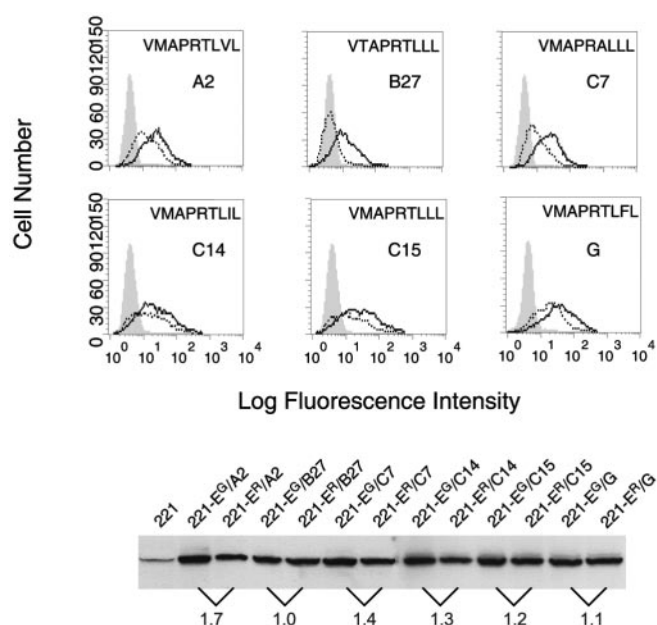


FIG. 1. Differential surface expression of HLA-E^G and HLA-E^R on transfected .221 cells. *Top*, hybrid cDNA constructs with various HLA-A, -B, -C, or -G leader peptides fused to each of the HLA-E^G and HLA-E^R mature protein coding sequences and cloned into vector pNS. Six pairs of constructs were transfected into class I negative 721.221 cells, and surface expression was assayed using anti-E-specific reagent 3D12 in FACS analysis. **Boldface traces** are from constructs made using the HLA-E^G coding sequence, and **dotted traces** represent constructs using the HLA-E^R coding sequence. *Shaded traces* represent isotype-matched control antibody staining either transfectant. The leader sequence used for each construct is indicated in the *upper right corner* of each histogram. *Bottom*, Western analysis performed on the 12 transfected cells and untransfected .221 cells showed relatively equal levels of HLA-E protein in each of the transfectants. Numerical ratios of densitometry tracings of the pairs connected by lines are indicated under the Western blot as HLA-E^G/HLA-E^R.

in B LCLs from individuals that were typed as HLA-E^R or -E^G homozygous in order to see whether these differences were reflected in normal cells (where more than one nonamer peptide might be available). After identifying several lines that were homozygous, they were further matched with regard to the nonamer peptides that were available for HLA-E binding. In some cases, this meant that the HLA-A, -B, and -C allotypes were the same, but in many cases these types were distinct, since the nonamers available for HLA-E binding are shared among several alleles and even between loci (e.g. HLA-A1 and -Cw14). Again, the relative differences in expression levels between the allelic variants were clearly evident; in each case, the E^G homozygous cells expressed higher levels of HLA-E complex (Fig. 2). There was some difference in the relative levels depending on the different mix of nonamer peptides available (e.g. compare A with B). To some degree, this was reflective of the relative differences found between the hybrid constructs and individual nonamers. However, it was interesting to find that not only the nonamer peptide but also the HLA-A, -B, and -C allotypes appeared to influence surface expression. The relative surface levels of the two alleles differed markedly, with highly similar HLA-A, -B, and -C alleles providing nonamer as shown in Fig. 2C (A*3201, B*4402, and C*0501 providing peptide to HLA-E^R and HLA-A*3303, B*44031, and C*1403 providing peptide to HLA-E^G). In contrast, a significantly narrower difference in surface expression levels was detected in Fig. 2D despite the fact that the same nonamers found in Fig. 2C pair were available for binding (HLA-E^R with HLA-A*0101, B*3701, and C*0602 *versus* HLA-A*2902, B*44031, and C*1601 with HLA-E^G-bearing LCLs).

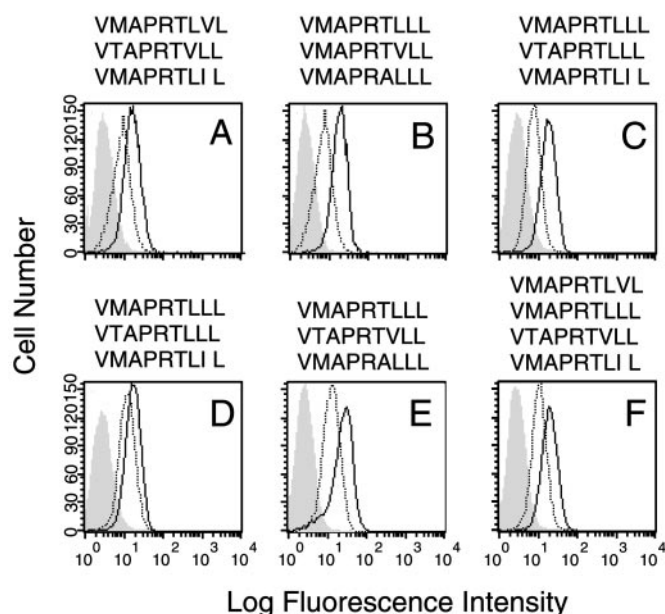


FIG. 2. Differential surface expression of HLA-E^G and HLA-E^R on LCLs expressing various HLA allotypes. Individuals and their corresponding LCLs for HLA-E^G or HLA-E^R as described (19). Cell lines were paired by choosing two LCLs that were homozygous for each of the HLA-E^G and HLA-E^R alleles and also had HLA-A, -B, and -C allotypes, which provided identical nonamer peptides to HLA-E. FACS analysis of five pairs of such LCLs are shown each stained with anti-E reagent 3D12. **Boldface traces** are from cells expressing only the HLA-E^G allele, whereas **dotted traces** are from cells expressing only the HLA-E^R allele. *Shaded traces* are from analysis using isotype-matched negative control antibody staining. The nonamer peptides derived from the HLA-A, -B, and -C allotypes and available to HLA-E for complex formation are listed above the corresponding FACS profile. The HLA types of the LCLs examined are as follows. *A*, HLA-E^R: A*0201, B*3501, and C*0401; HLA-E^G: A*6802, B*5301, and C*0401. *B*, HLA-E^G: A*0101, B*0801, and C*0701; HLA-E^R: A*0101, B*0801, and C*0701. *C*, HLA-E^R: A*3201, B*4402, and C*0501; HLA-E^G: A*3303, B*44031, and C*1403. *D*, HLA-E^R: HLA-A*0101, B*3701, and C*0602; HLA-E^G: HLA-A*2902, B*44031, and C*1601. *E*, HLA-E^R: A*0101, B*4101, and C*1801; HLA-E^G: A*0101, B*4901, and C*0701. *F*, HLA-E^R: A*0202/A*1101, B*1501/B*3501, and C*0401/C*0303; HLA-E^G: A*2403/A*3303, B*4601/B*1512, and C*0102/C*03.

Measuring Differential Peptide Affinity for HLA-E^R and -E^G—As one of three required components for folding a functional class I molecule, peptide has the ability to alter complex formation through the binding energy available, through its interaction with heavy chain, to stabilize the folded structure. Therefore, peptide affinity is indirectly reflected by complex folding efficiency. We used a qualitative measurement, based on the ability of peptide at different concentrations to drive the formation of complex in a refolding mixture as described (28), as an estimate of the affinity for different peptides of the E^G and E^R alleles. The results of this experiment, using seven distinct nonamer peptides, are shown in Fig. 3, where increasing peptide concentrations are titrated against constant levels of each of the two allelic heavy chains and β_2m . In each case, the relative affinity of the E^G heavy chain for peptide was significantly greater than that of E^R, largely reflecting the relative differences found in surface levels when single allele-peptide combinations were examined (Fig. 1). The most dramatic effect was seen using the HLA-B27-derived nonamer, where little complex could be formed with the E^R heavy chain even at high peptide concentrations. Higher (but still relatively low) affinity for the E^G allele was apparent, although at high concentrations both complexes could be refolded and intact complex isolated (see below for stability measurements).

The relative difference in peptide concentration required to achieve refolding of the two alleles was substantial as meas-

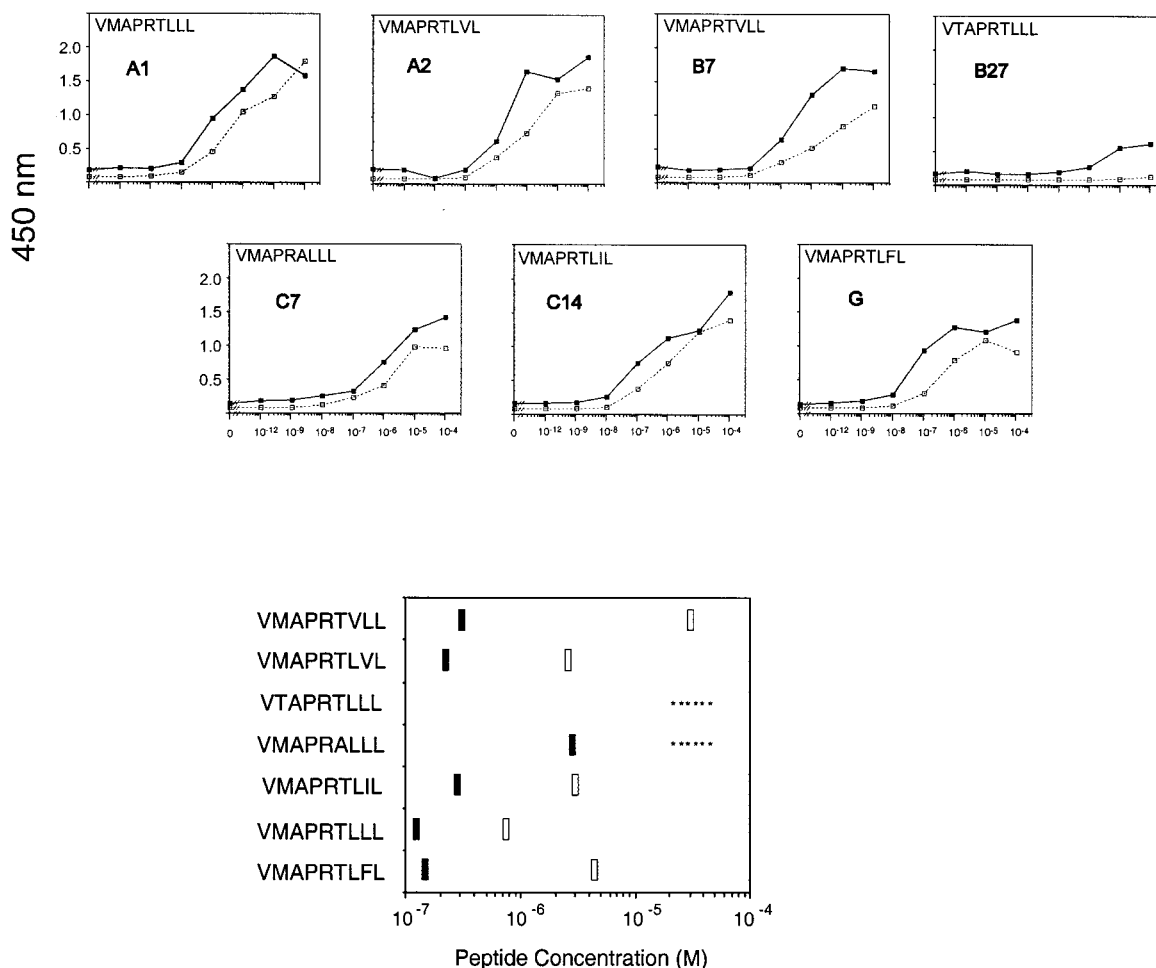


FIG. 3. **Differential peptide affinity for HLA-E^G and HLA-E^R.** *Top*, the results of enzyme-linked immunosorbent assay using antibodies 3D12 plate-bound and peroxidase-conjugated rabbit anti-human β_2m (Dako) to assay refolded material are diagrammed for each of seven pairs of refolding experiments. The concentration required for refolding was quantified and compared with maximum assembly achieved using 100 μ M VMAPRTLVL. Relative amounts are indicated on the vertical axis, and the logarithmic scale of peptide concentrations is indicated on the horizontal axis. The peptide used in each refolding is indicated in the upper left corner of the graph, and the HLA allele from which the sequence was derived is indicated immediately below. *Bottom*, comparison of median peptide concentrations required for HLA-E^G and HLA-E^R complex refolding. The concentration of peptide required to refold 50% of the HLA-E complex is presented for each of the peptide and HLA-E^G and HLA-E^R heavy chain combinations. Peptide sequences used are indicated at the left of the graph. *Solid bars* indicate results using the HLA-E^G heavy chain, and *open bars* indicate HLA-E^R refolding results. The *asterisks* indicate that the tested peptide concentrations did not achieve median refolding levels.

ured by the point at which 50% of heavy chain was converted to refolded complex (Fig. 3). Differences of over 2 orders of magnitude were apparent between alleles when the B7-derived nonamer VMAPRTVLL was used. Smaller relative differences were seen for other nonamers, varying from 7-fold to over 14-fold. The two poorest drivers of refolded complex formation were the Cw7- and the B27-derived nonamers; the latter was shown to yield relatively low levels of the HLA-E^G complex on the cell surface and almost nonexistent surface levels of the HLA-E^R complex. Interestingly, when the HLA-Cw7-derived nonamer is complexed with HLA-E (either allele), the complex formed is not functional in the interaction between HLA-E and CD94-NKG2A despite promoting the formation of stable surface-expressed HLA-E (14).

Thermal Stability of HLA-E in Complex with Different Peptides by CD—In order to assess the effect of substitutions at position 107 or in the bound peptide on the thermal stability of HLA-E, we determined the melting transition temperature (T_m) by following the thermal denaturation of different HLA-E-peptide complexes by CD spectroscopy (see Fig. 4). Three different peptides were used in these experiments, derived from the leader peptides of HLA-B7 (VMAPRTVLL), HLA-B27

(VTAPRTLLL), and HLA-G (VMAPRTLFL). Data were also collected from “empty” HLA-E molecules refolded in the absence of added peptides. Prior studies have shown that classical MHC class I proteins (H-2K^d) have T_m values in the range of 52–61 °C depending upon the peptide used, whereas “empty” molecules have a T_m of 45 °C (36, 37). In these experiments, the HLA-G- and HLA-B7-derived peptides yield identical T_m values when bound by either HLA-E^G ($T_m = 52$ °C) or HLA-E^R ($T_m = 49$ °C), suggesting that these substitutions at positions P7 and P8 do not affect stability. This is consistent with the results of the crystallographic analyses; the residue at P7 is either of the relatively conservative pair of valine or leucine, with the small movements at the C α of this peptide residue (<1 Å) correlated more with which position the molecule occupies in the asymmetric unit and not with the identity of the P7 residue (see below); the side chain of residue P8 extends into solvent. HLA-E^G-peptide complexes uniformly display higher T_m values than the corresponding HLA-E^R complexes: 52 °C for the HLA-E^G-B7 complex *versus* 49 °C for the HLA-E^R-B7 complex, and 49 °C for the HLA-E^G-B27 complex *versus* 43 °C for the HLA-E^R-B27. This relationship holds true for the T_m values of the “empty” molecules: HLA-E^G-empty (44 °C) *versus* HLA-E^R-

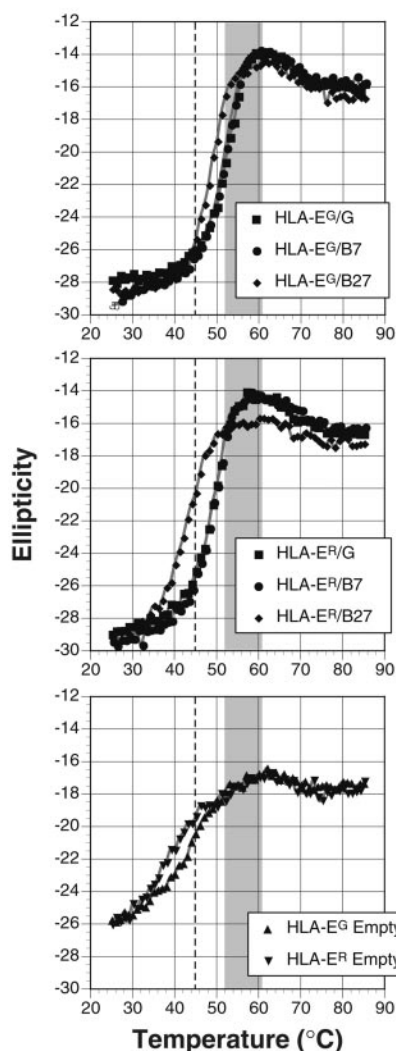


FIG. 4. **Thermal denaturation curves for HLA-E molecules.** Shown are plots of ellipticity (monitored at 219 nm) versus temperature for the unfolding transition of HLA-E^G refolded with three different peptides (*top panel*); HLA-E^R refolded with three different peptides (*middle panel*); and HLA-E^G and HLA-E^R refolded in the absence of added peptide (*bottom panel*). Each curve represents the average of three separate denaturations. The gray band indicates the range of T_m values reported for different classical MHC class I-peptide complexes, and the dashed line indicates the T_m of an “empty” complex (36, 37).

empty (40 °C). We would argue that even these relatively modest differences in T_m are significant, given the quality of the data as evidenced by the nearly complete overlap of the G and B7 peptide curves.

Crystallographic Analysis of HLA-E^G—In order to determine the structural consequences of (i) the arginine-to-glycine substitution at position 107 and (ii) the substitutions present in different HLA leader-derived peptides presented by HLA-E, we determined the structures of HLA-E^G in complex with two different peptides by x-ray crystallography: VMAPRTVLL (derived from the HLA-B7 leader) and VTAPRTLIII (derived from the HLA-B27 leader). The structures were determined at resolutions of 2.8 and 3.1 Å, respectively, using the previously determined HLA-E^R-B7 crystal structure (38) as an initial phasing model. Since there are two molecules per asymmetric unit for each of the three complexes, which we refer to as positions 1 and 2, together these analyses yield a total of six independent views of the HLA-E structure. Great care was taken during the E^G refinements to minimize model bias, including the stringent use of composite omit maps in the initial phases of rebuilding.

The crystallographic analysis revealed the expected, classic MHC class I fold (39), with the heavy chain, or α -chain, folded into the peptide-binding $\alpha 1\alpha 2$ platform domain and immunoglobulin-like $\alpha 3$ domain, associated with the invariant, immunoglobulin-like light chain (β_2m ; see Fig. 5A). The six independent views of the HLA-E structure are all extremely similar, with pairwise superposition root mean square deviations, calculated on all common C α s, of between 0.11 and 0.85 Å (Table I). The most pairwise similar models are the E^G-B7 and E^G-B27 molecules sitting at position 1 in the two different E^G asymmetric units, followed closely by the E^G-B7 and E^G-B27 molecules sitting at position 2; the largest differences occur between the molecules at position 1 or 2 in either of the two E^G structures. The two E^R-B7 molecules (positions 1 and 2) are much more similar to each other than either pair of E^G molecules (positions 1 and 2) because of the application of much tighter noncrystallographic symmetry restraints in the E^R analysis. Differences in E^G structures at the two positions in the asymmetric unit reflect, in part, the affect of the different crystal environments at the two positions on flexible loops and side chains of solvent-exposed residues. Differences between E^G and E^R structures are probably somewhat influenced by the slight differences in the crystallization regimens.

The largest differences among the HLA-E structures (Fig. 5A) occur at the loop corresponding to the region of classical MHC class I proteins associated with CD8 binding (residues 222–229) (40). The backbone of this loop moves by up to 4.6 Å between matching C α s between the molecules at positions 1 and 2 in the two E^G complex structures, although this loop retains a similar conformation in both molecules at either position 1 or 2 in the two structures. The loop adopts a similar conformation in both E^R molecules (positions 1 and 2), again probably due to the tighter noncrystallographic symmetry restraints, intermediate between the conformation seen in either of the molecules at position 1 or 2 in the E^G structures. When the CD8 loops (residues 216–230) are excluded from pairwise superpositions, the root mean square deviation values fall to between 0.50 and 0.66 Å. There are less dramatic differences in the loops formed by residues 133–139 and residues 193–199. However, the CD8 binding loop and the 133–139 loop are involved in crystal contacts; therefore, these loops may be best described as conformationally ill defined, or flexible, loops that have the particular conformations observed in the crystal structures selected by packing interactions and/or the particular crystallization/cryopreservation conditions. Our analysis therefore suggests that the failure of HLA-E to bind CD8 is not strictly due to constraints holding this loop in a nonbinding conformation imposed in the context of the HLA-E heavy chain.

Structural Affect of the Gly/Arg Allelic Substitution—The arginine-to-glycine substitution has a very limited effect on the structure of HLA-E; the C α positions of residues 104–109 are within 0.8 Å of each other among the six different structures, and the side chains adopt comparable rotamers and conformations. This substitution does result in the elimination of a hydrogen bond between the side chains of Arg¹⁰⁷ and His³ and in the apparent, slight rearrangement of the hydrogen bond network around the residues surrounding position 107 in the E^R versus E^G structures (Fig. 5B). However, structural changes in this neighborhood are more dramatic between the molecules at positions 1 and 2 in the E^G structures than between corresponding E^G and E^R structures, suggesting that these residues are more strongly affected by the crystal environment (residue 107 lies in a loop contacting the $\alpha 3$ domain of a neighboring molecule) than by the arginine-to-glycine substitution.

The residue at position 107 in HLA-E is not expected to directly or indirectly affect the interaction with NKG2-CD94

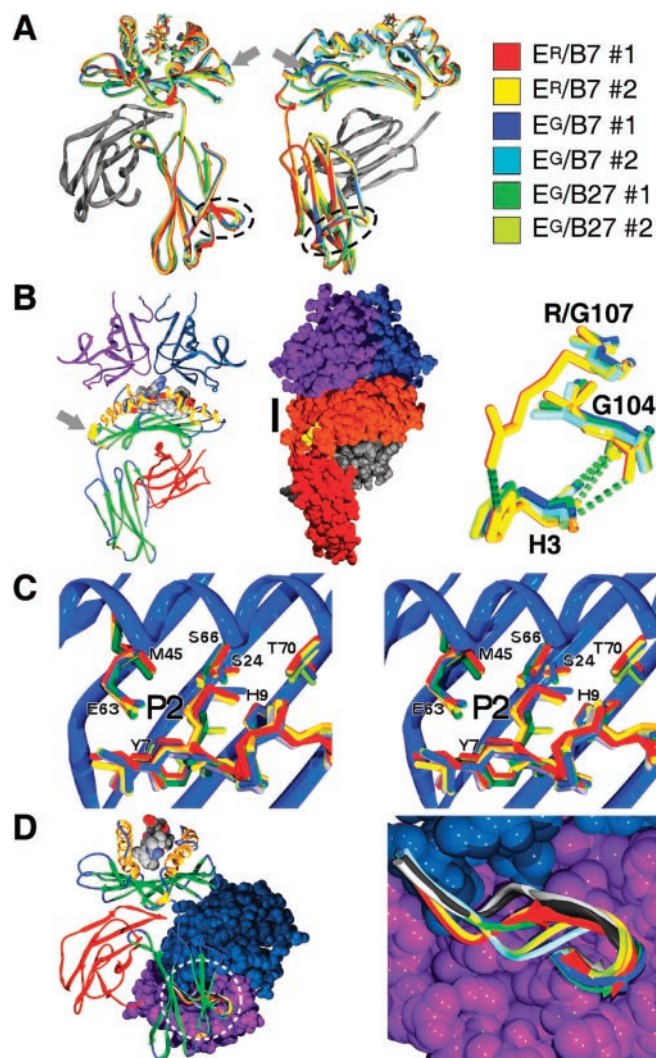


FIG. 5. Structures of HLA-E in complex with different peptides. *A*, two orthogonal views (left and middle) of the superposition of ribbon representations of the six different HLA-E crystal structures are shown, colored as indicated (right), with β_2m shown in gray. β -Strands are shown as arrows, and α -helices are shown as coils; the bound peptides are shown in stick style. The two molecules of HLA-E^R are from PDB file 1mhe (38); the four HLA-E^G molecules are from the two independent crystal structures reported here. The arrows indicate the position of residue 107, with its C α shown as a sphere. The CD8 loops are circled. *B*, a ribbon representation of the proposed model of the NKG2A-CD94-HLA-E complex (41) is shown on the left. The HLA-E α chain is colored by secondary structure (yellow, α -helix; green, β -strands; blue, coil), β_2m is colored red, CD94 is colored purple, and NKG2A is colored blue. β -Strands are shown as arrows, and α -helices are shown as coils; the bound peptide is shown in space-filling style colored by atom type (carbon (gray), oxygen (red), nitrogen (blue), and sulfur (yellow)). An arrow indicates the position of residue 107 (yellow spheres). In the middle, rotated by 30° around the vertical axis relative to the view on the left, the NKG2A-CD94-HLA-E complex model is shown in space-filling style, colored by domain (NKG2A (blue), CD94 (purple), $\alpha 1\alpha 2$ platform (orange), $\alpha 3$ (red), and β_2m (gray)). Arg¹⁰⁷ is colored yellow. The bar spans the 12-Å distance between the nearest atoms of CD94 and Arg¹⁰⁷. On the right is shown a detailed view, in stick style and colored as in *A*, of the interactions residue 107 makes with its neighbors in the six HLA-E structures. Hydrogen bonds are shown as dotted green lines. The orientation of the detail view is similar to that of the middle view. *C*, a stereoview of the P2 binding pocket is shown, with the backbone ribbon of one HLA-E^G structure, colored blue, and the side chains of residues lining the P2 pocket (in stick style) from all six different HLA-E structures, colored as in *A*. The side chains and the P2 peptide residue are labeled. *D*, left, a representation of the HLA-A2-CD8 $\alpha\alpha$ complex structure (PDB file 1ajk (40)) is shown, with HLA-A2 shown in a ribbon representation as in *B* and with the two domains of CD8 shown in space-filling style and colored either blue or purple. The CD8 α binding loops (residues 222–229, within the white

heterodimeric receptors on the basis of a model of the NKG2A-CD94-HLA-E complex derived from the structure of the NKG2D-MICA NK cell receptor-ligand complex (41). In this model (see Fig. 5B), CD94 overlies the $\alpha 1$ domain of HLA-E, with a small hydrophobic patch on CD94 (Phe¹¹⁴ and Leu¹⁶²) matching a similar patch on HLA-E (Ile⁷³, Val⁷⁶, and the side chain of the P8 residue in the peptide, leucine in the crystal structure). There is no comparable hydrophobic patch on the $\alpha 2$ domain of HLA-E underlying the presumed position of the NKG2 moiety, but Phe¹¹⁴ and Leu¹⁶² are replaced with serine and lysine, respectively, in the sequences of both NKG2A and NKG2C, thus accommodating this change. The $\beta 6$ strand and the $\beta 6/\beta 7$ loop in CD94 are dominated by four acidic residues (Asp¹⁶³, Asp¹⁶⁸, Glu¹⁶⁴, and Glu¹⁶⁷) that match a cluster of charged residues on HLA-E (Asp⁶⁹, Arg⁷⁵, Lys¹⁴⁶, and Arg^{P5}). The binding site on NKG2A is dominated by charged and polar residues (Glu⁵⁸, Arg⁶², Arg⁶⁵, His¹⁵⁵, Asp¹⁶², Glu¹⁶⁶, and Lys¹⁷⁰), which would overlie a similarly charged surface on HLA-E (Arg⁷⁵, Arg⁷⁹, Arg⁸², and Gln⁷²). The side chain of the arginine at the P5 position in the peptide would be able to exchange hydrogen bonds with residues from either NKG2 or CD94 at the homodimer interface. Gln¹¹² in the $\beta 2/\alpha 1$ loop of CD94 is in position to reach into the peptide binding groove, hydrogen-bonding to the peptide backbone at either P4 or P5. In this model, no atom in any allowed conformation of the side chain of an arginine at position 107 approaches closer than 9 Å to any atom in NKG2A.

Effect of Different Peptides on Structure—The HLA-E structure is even less affected by the methionine-to-threonine substitution between the HLA-B7- and HLA-B27-derived peptides at the P2 position (see Fig. 5C) or the leucine-to-valine substitution at the P7 position. There are no significant conformational differences among HLA-E residues lining the corresponding pockets for these peptide residues. There are *minor* differences in the side chain of Ser²⁴ in the P2 pocket, which adopts different rotamers in the HLA-E^R versus the HLA-E^G structures, although these differences may be the result of different interpretations of moderate resolution electron density maps. The methionine-to-threonine substitution at P2 does increase the volume of a cavity, located adjacent to the P2 side chain, from ~31 to 53 Å³, a direct consequence of the smaller size of the threonine side chain and the lack of compensating rearrangements of pocket residues. Such cavities have been directly linked to protein stability in other studies (42), and this is the likeliest explanation for the effect different peptides have on HLA-E stability (see below).

DISCUSSION

In the present study, we opened a thorough investigation of the biochemical differences between the two nonsynonymous HLA-E alleles. This study was motivated primarily by our initial observation that, in most cases, the HLA-E^G allele was expressed at higher levels than the HLA-E^R allele in human transfected cells regardless of which peptide was bound. This observation was confirmed by a similar comparative analysis of HLA-E expression on normal cells, where, to a degree depending on the available classical class I signal sequences, the HLA-E^G allele was expressed at significantly higher levels. Since studies have suggested that cell surface levels of HLA-E can affect the signaling through CD94-NKG2 (3, 14, 43), such a physical difference in cell surface expression levels might be

dashed circle) from all six HLA-E structures (colored as in *A*) and the H-2K^b-CD8 $\alpha\alpha$ complex structure (gray; PDB file 1bqh) are superimposed on the HLA-A2-CD8 $\alpha\alpha$ complex structure (loop colored black). *Right*, a detailed view of the CD8 $\alpha\alpha$ loops is shown.

translated into functional differences between these molecules. An additional dimension of complexity is introduced by the identity of the bound peptide and the particular allele, since such functional differences have been demonstrated to depend on these factors for HLA-E (14).

We first considered the possibility that the substitution of glycine for arginine at position 107 would result in structural differences between the two alleles, and since the crystal structure of HLA-E^R had been solved (38), we undertook the crystallographic analysis of HLA-E^G complexed with two different peptides. However, the structures of the peptide-binding, $\alpha 1\alpha 2$ platform domains of HLA-E with either peptide bound to either of the two alleles are essentially identical within the accuracy of the analysis. Therefore, the structures do not immediately provide an explanation for the significant difference in the stability of the two alleles. The one structural difference that is observed between HLA-E^G and HLA-E^R is the presence of an additional hydrogen bond in the HLA-E^R molecule involving the side chain of arginine 107, although this might naively imply that the HLA-E^G allele would be less stable than the HLA-E^R allele, the opposite of what is observed. Likewise, the presence of an additional glycine in the HLA-E sequence would be predicted to result in a larger loss of entropy during folding, destabilizing the HLA-E^G structure relative to HLA-E^R, again the opposite of what is observed.

Direct effects on stability, and thus indirect effects on cell-surface half-life and peptide or receptor affinity, can be explained by the gain or loss of stabilizing interactions between HLA-E alleles and the various bound peptides. Differences in the identity of the P2 residue of the peptide result in cavities within the peptide-platform domain complex structure by varying the quality of fit of the different peptides into an apparently rigid protein structure. The relative quality of the fit of peptide into platform correlates well with the differences in thermal stability and cell surface expression levels measured for HLA-E complexes with different peptides. As a consequence, each allele shows differing affinities with distinct peptides in a manner that correlates with the differing stability. The HLA-B27-derived nonamer provides a striking example of this difference. The HLA-E^G heavy chain does form complexes with the B27 nonamer, albeit at relatively high concentrations, whereas the HLA-E^R molecule does not bind the nonamer under the conditions tested. This is reflected precisely in surface expression using the hybrid constructs with the B27 signal sequence fused to either HLA-E allele, where no detectable HLA-E^R was observed on the surface of 221 transfectants, whereas significant levels of surface HLA-E^G were observed under the same conditions, and in T_m measurements, where the stability of HLA-E^R refolded in the presence of the B27 peptide is comparable with peptideless MHC class I proteins.

The stability of the complexes was also consistent with a melting temperature of some 5 °C higher for the HLA-E^G/B27 nonamer complex. Indeed, with all peptides tested, completely consistent differences were observed between the alleles among all three measures of cell surface expression level, peptide affinity, and complex stability. Thus, the differences in expression levels are not due exclusively to the affinities for available peptide or to any other single factor, but instead are due to the interrelated combination of relative affinity and stability of the refolded complex. The measurements of stability show clearly that the E^G complex has a significantly higher melting temperature over E^R regardless of the peptide bound. Further, it is unlikely that peptide is limiting, since classical class I molecules, the source of peptide, are over 20-fold more abundant than the HLA-E complex (13). Further, previous peptide feed-

ing experiments had indicated that steady state HLA-E levels were controlled by the half-life of the complex and not by limiting peptide (3, 14).

Although these studies implicate differing surface levels of HLA-E as a possible modulator of ligand interaction, we have not ruled out an effect of the substitution at residue 107 as altering an interaction between HLA-E and CD94-NKG2. In experiments carried out with transfectants *in vitro*, essentially similar results were observed regardless of the HLA-E allele used (3). Nevertheless, subtle effects that may have significance *in vivo* would probably not be detected in these experiments. However, no differences were observed in comparisons of HLA-E^G and HLA-E^R structures that would directly or indirectly affect the interaction with NKG2-CD94 heterodimers. The possibility that TCRs recognize HLA-E directly (44) adds the possibility that this position affects interactions with receptors other than NKG2-CD94. Therefore, it is at least conceivable that the allelic variation has two effects on ligand interaction, one determining quantitative differences in the amount of HLA-E complexes on the cell surface at any given time and the second distinguishing the molecules qualitatively through alterations in the effective affinity for interacting receptors.

The level of selection acting on the HLA-E locus to balance these alleles in the population is not entirely clear, although at least two possibilities can be envisioned. Whereas the present study was limited to an examination of HLA class I signal sequence-derived peptides, TCR-derived peptides have been reported to bind and be presented by HLA-E (45). If, as these studies suggest, HLA-E does prove to be involved in TCR V β peptide presentation, the likelihood that these peptides show differential binding between the two alleles seems plausible. Indeed, of the seven peptides tested, in every case the relative affinity of peptide was higher for HLA-E^G (Fig. 3). Evidence for pathogen-derived peptides binding and being presented by HLA-E has also been suggested (46), and evidence for recognition of HLA-E by TCR α/β seems to support such a possibility (44). It therefore is conceivable that selection for maintenance of two HLA-E alleles could be acting at the level of regulation of peripheral T cell function, of pathogen-mediated immune recognition, or both.

Alternatively, an additional and significant level of balancing selection might operate via HLA-E expression in the placenta. Several facts go together to implicate this as a mechanism for a relatively rapid stabilization of a new allele in a population. First, placental trophoblasts expressing HLA-G also express HLA-E complexed with the HLA-G nonamer (47). A relatively large difference in binding affinity, derived from the differential ability of peptide to foster protein folding, between HLA-E^G and HLA-E^R for the HLA-G nonamer was observed (Fig. 3), suggesting a relative difference in surface expression levels between these alleles in the placenta. Since the HLA-E/G nonamer complex can evoke an inhibitory or stimulatory response from NK cells (14) and since relative surface levels are likely to directly influence the efficiency of either inhibition or stimulation via CD94-NKG2, it is plausible that there is significant room for modulation of function in the arena of the maternal-placental immune interaction. Indeed, a unique NK response is associated with pregnancy (48), and rather than acting to inhibit NK activity in the maternal decidua, HLA-E may indeed act to stimulate NK to secrete cytokines appropriate for a stable immunological environment. The proper balance of inhibition and stimulation to yield a stable pregnancy may require higher or lower levels of HLA-E, depending upon other immunological and genetic factors present, thus conceivably providing strong selection on a newly introduced HLA-E allele.

Acknowledgments—We thank Robert Fleming-Jones for assistance with crystallization and L. Hung, G. McDermott and T. Earnest (Advanced Light Source, Lawrence Berkeley National Laboratory) for assistance with data collection. The outstanding technical assistance of Mark Morris is gratefully acknowledged.

REFERENCES

1. Townsend, A., and Bodmer, H. (1989) *Ann. Rev. Immunol.* **7**, 601–624
2. Geraghty, D. E., Koller, B. H., Hansen, J. A., and Orr, H. T. (1992) *J. Immunol.* **149**, 1934–1946
3. Lee, N., Llano, M., Carretero, M., Ishitani, A., Navarro, F., Lopez-Botet, M., and Geraghty, D. E. (1998) *Proc. Natl. Acad. Sci. U. S. A.* **95**, 5199–5204
4. Kovats, S., Main, E. K., Librach, C., Stubblebine, M., Fisher, S. J., and DeMars, R. (1990) *Science* **248**, 220–223
5. Geraghty, D. E., Wei, X. H., Orr, H. T., and Koller, B. H. (1990) *J. Exp. Med.* **171**, 1–18
6. Lepin, E. J., Bastin, J. M., Allan, D. S., Roncador, G., Braud, V. M., Mason, D. Y., van der Merwe, P. A., McMichael, A. J., Bell, J. I., Powis, S. H., and O'Callaghan, C. A. (2000) *Eur. J. Immunol.* **30**, 3552–3561
7. Braud, V. M., Allan, D. S., O'Callaghan, C. A., Soderstrom, K., D'Andrea, A., Ogg, G. S., Lazetic, S., Young, N. T., Bell, J. I., Phillips, J. H., Lanier, L. L., and McMichael, A. J. (1998) *Nature* **391**, 795–799
8. Aramburu, J., Balboa, M. A., Izquierdo, M., and Lopez-Botet, M. (1991) *J. Immunol.* **147**, 714–721
9. Aramburu, J., Balboa, M. A., Ramirez, A., Silva, A., Acevedo, A., Sanchez-Madrid, F., De Landazuri, M. O., and Lopez-Botet, M. (1990) *J. Immunol.* **144**, 3238–3247
10. Bellon, T., Heredia, A. B., Llano, M., Minguela, A., Rodriguez, A., Lopez-Botet, M., and Aparicio, P. (1999) *J. Immunol.* **162**, 3996–4002
11. Lazetic, S., Chang, C., Houchins, J. P., Lanier, L. L., and Phillips, J. H. (1996) *J. Immunol.* **157**, 4741–4745
12. Perez-Villar, J. J., Melero, I., Rodriguez, A., Carretero, M., Aramburu, J., Sivori, S., Orengo, A. M., Moretta, A., and Lopez-Botet, M. (1995) *J. Immunol.* **154**, 5779–5788
13. Lee, N., Goodlett, D. R., Ishitani, A., Marquardt, H., and Geraghty, D. E. (1998) *J. Immunol.* **160**, 4951–4960
14. Llano, M., Lee, N., Navarro, F., Garcia, P., Albar, J. P., Geraghty, D. E., and Lopez-Botet, M. (1998) *Eur. J. Immunol.* **28**, 2854–2863
15. Little, A. M., and Parham, P. (1999) *Rev. Immunogenet.* **1**, 105–123
16. Hughes, A. L., and Nei, M. (1988) *Nature* **335**, 167–170
17. Geraghty, D. E., Stockscheider, M., Ishitani, A., and Hansen, J. A. (1992) *Hum. Immunol.* **33**, 174–184
18. Matte, C., Lacaille, J., Zijenah, L., Ward, B., and Roger, M. (2000) *Hum. Immunol.* **61**, 1150–1156
19. Grimsley, C., Kawasaki, A., Gassner, C., Sageshima, N., Nose, Y., Hatake, K., Geraghty, D. E., and Ishitani, A. (2002) *Tissue Antigens* **60**, 206–212
20. Grimsley, C., and Ober, C. (1997) *Hum. Immunol.* **52**, 33–40
21. Schatz, P. J. (1993) *Bio/Technology* **11**, 1138–1143
22. MacFerrin, K. D., Terranova, M. P., Schreiber, S. L., and Verdine, G. L. (1990) *Proc. Natl. Acad. Sci. U. S. A.* **87**, 1937–1941
23. Griffin, T. A., Yuan, J., Friede, T., Stevanovic, S., Ariyoshi, K., Rowland-Jones, S. L., Rammensee, H. G., and Colbert, R. A. (1997) *J. Immunol.* **159**, 4887–4897
24. Garbocki, D. N., Hung, D. T., and Wiley, D. C. (1992) *Proc. Natl. Acad. Sci. U. S. A.* **89**, 3429–3433
25. O'Callaghan, C. A., Tormo, J., Willcox, B. E., Blundell, C. D., Jakobsen, B. K., Stuart, D. I., McMichael, A. J., Bell, J. I., and Jones, E. Y. (1998) *Protein Sci.* **7**, 1264–1266
26. Fujii, T., Ishitani, A., and Geraghty, D. E. (1994) *J. Immunol.* **153**, 5516–5524
27. Mazda, O., Satoh, E., and Imanishi, J. (1997) *Scand. J. Immunol.* **46**, 262–267
28. Sylvester-Hvid, C., Kristensen, N., Blicher, T., Ferre, H., Lauemoller, S. L., Wolf, X. A., Lamberth, K., Nissen, M. H., Pedersen, L. O., and Buus, S. (2002) *Tissue Antigens* **59**, 251–258
29. Otwinowski, Z., and Minor, W. (1997) *Methods Enzymol.* **276**, 307–326
30. Berman, H. M., Westbrook, J., Feng, Z., Gilliland, G., Bhat, T. N., Weissig, H., Shindyalov, I. N., and Bourne, P. E. (2000) *Nucleic Acids Res.* **28**, 235–242
31. Brünger, A. T., Adams, P. D., Marius Clore, G., DeLano, W. L., Gros, P., Grosse-Kunstleve, R. W., Jiang, J.-S., Kuszewski, J., Nilges, M., Pannu, N. S., Read, R. J., Rice, L. M., Simonson, T., and Warren, G. L. (1998) *Acta Crystallogr. Sec. D* **54**, 905–921
32. McRee, D. E. (1992) *J. Mol. Graphics* **10**, 44–46
33. Brünger, A. T. (1992) *Nature* **355**, 472–475
34. Kleywegt, G. J., and Brünger, A. T. (1996) *Structure* **4**, 897–904
35. Ulbrecht, M., Couturier, A., Martinuzzi, S., Pla, M., Srivastava, R., Peterson, P. A., and Weiss, E. H. (1999) *Eur. J. Immunol.* **29**, 537–547
36. Fahnestock, M. L., Tamir, I., Narhi, L., and Bjorkman, P. J. (1992) *Science* **258**, 1658–1662
37. Morgan, C. S., Holton, J. M., Olafson, B. D., Bjorkman, P. J., and Mayo, S. L. (1997) *Tissue Antigens* **6**, 1771–1773
38. O'Callaghan, C. A., Tormo, J., Willcox, B. E., Braud, V. M., Jakobsen, B. K., Stuart, D. I., McMichael, A. J., Bell, J. I., and Jones, E. Y. (1998) *Mol. Cell* **1**, 531–541
39. Bjorkman, P. J., and Parham, P. (1990) *Annu. Rev. Biochem.* **90**, 253–288
40. Gao, G. F., Tormo, J., Gerth, U. C., Wyer, J. R., McMichael, A. J., Stuart, D. I., Bell, J. I., Jones, E. Y., and Jakobsen, B. K. (1997) *Nature* **387**, 630–634
41. Li, P., Morris, D. L., Willcox, B. E., Steinle, A., Spies, T., and Strong, R. K. (2001) *Nat. Immunol.* **2**, 443–451
42. Xu, J., Baase, W. A., Baldwin, E., and Matthews, B. W. (1998) *Protein Sci.* **7**, 158–177
43. Vales-Gomez, M., Reyburn, H. T., Erskine, R. A., Lopez-Botet, M., and Strominger, J. L. (1999) *EMBO J.* **18**, 4250–4260
44. Pietra, G., Romagnani, C., Falco, M., Vitale, M., Castriconi, R., Pende, D., Millo, E., Anfossi, S., Biassoni, R., Moretta, L., and Mingari, M. C. (2001) *Eur. J. Immunol.* **31**, 3687–3693
45. Li, J., Goldstein, I., Glickman-Nir, E., Jiang, H., and Chess, L. (2001) *J. Immunol.* **167**, 3800–3808
46. Ulbrecht, M., Modrow, S., Srivastava, R., Peterson, P. A., and Weiss, E. H. (1998) *J. Immunol.* **160**, 4375–4385
47. Ishitani, A., Sageshima, N., Lee, N., Dorofeeva, N., Hatake, K., H., M., and Geraghty, D. E. (2003) *J. Immunol.*, in press
48. King, A., Burrows, T., Verma, S., Hiby, S., and Loke, Y. W. (1998) *Hum. Reprod. Update* **4**, 480–485
49. Laskowski, R. A., MacArthur, M. W., Hutchinson, E. G., and Thornton, J. M. (1992) *J. Appl. Crystallogr.* **26**, 283–291